ISSN 1070-3632, Russian Journal of General Chemistry, 2013, Vol. 83, No. 11, pp. 2167–2172. © Pleiades Publishing, Ltd., 2013.
Original Russian Text © G.A. Emel'chenko, V.M. Masalov, A.A. Zhokhov, A.N. Tereshchenko, E.A. Shteinman, V.I. Zinenko, I.I. Khodos, Yu.A. Agafonov, 2012, published in Rossiiskii Khimicheskii Zhurnal, 2012, Vol. 56, Nos. 1–2, pp. 44–49.

Carbon and Carbon–Silicon Carbide Nanocomposites with Inverse Opal Structure

G. A. Emel'chenko[a], V. M. Masalov[a], A. A. Zhokhov[a], A. N. Tereshchenko[a], E. A. Shteinman[a], V. I. Zinenko[b], I. I. Khodos[b], and Yu. A. Agafonov[b]

[a] *Institute of Solid State Physics Federal State Budgetary Research Institution, Russian Academy of Sciences, ul. Akademika Osip'yna 2, Chernogolovka, Moscow oblast, 142432 Russia*
e-mail: emelch@issp.ac.ru

[b] *Institute of Microelectronics Technology and High-Purity Materials Federal State Budgetary Research Institution, Russian Academy of Sciences, ul. Akademika Osip'yna 6, Chernogolovka, Moscow oblast, 142432 Russia*

Received June 1, 2012

Abstract—Synthesis, morphology, and structural characteristics of carbon and SiC/C nanocomposites with a lattice of inverse opal were investigated. Porous structure characteristics were determined by gas adsorption–desorption. Photoluminescence of SiC/C nanocomposites, induced by implantation of helium ions, and their structure revealed by high-resolution transmission electron microscopy were studied.

DOI: 10.1134/S1070363213110364

INTRODUCTION

Nanostructured carbon materials have found wide application in technics. The most active R&D work has been on the application of such materials in portable power sources for microelectronics, as well as accumulators, pulse force devices, and other equipment which requires high-speed power sources. The key structural parameters of nanosized carbon materials for application as electrodes in chemical power sources are the specific surface area and the pore size and topology. An inter-related system of micro- and meso-pores in combination with a large surface area of electrodes favors higher performance characteristics of such devices.

Template synthesis of nanostructured carbon materials offers the greatest possibilities for controlling the pore structure of a material, compared to other synthesis technologies. This technology is based on embedding of a substance with a perfect crystal lattice into voids in natural or artificial crystalline templates, for example, opals.

In the present work we studied the effect of thermochemical treatment of opal matrices filled with carbon compounds followed by removal of silicon dioxide on the porous structure of the resulting materials. The porous structure parameters were determined by gas adsorption–desorption. Photoluminescence of the SiC/C nanocomposites, induced by implantation of helium ions, and their structure revealed by high-resolution transmission electron microscopy were studied.

EXPERIMENTAL

Carbon nanostructures with an inverse opal crystal lattice were obtained using opal templates prepared by sedimentation of suspensions of monodisperse colloidal SiO_2 particles with diameters ranging from 10 nm to 300 nm. Smaller colloidal particles (< 100 nm) were precipitated by centrifuging. Carbon was introduced into an opal template by impregnating it with an aqueous sugar solution doped with sulfuric acid. Samples were kept in the sugar solution at 100°C for ~5 h and then were taken out and dried (160°C, 18 h). The impregnation and thermal treatment operations were repeated, after which the samples were annealed under argon in the following conditions: 600°C, 3 h for opals with an average particle size of 10–15 nm; 900°C, 3 h for opals with an average particle size of 50–80 nm; and 1500°C, 3 h, vacuum, for opals with an average particle size of 250–300 nm.

The resulting carbon-filled opal matrices were activated in an alkaline solution and dried at 60°C for 2 h and then at 110°C for 12 h. Carbonization was performed at 800°C in an inert atmosphere for 2 h,

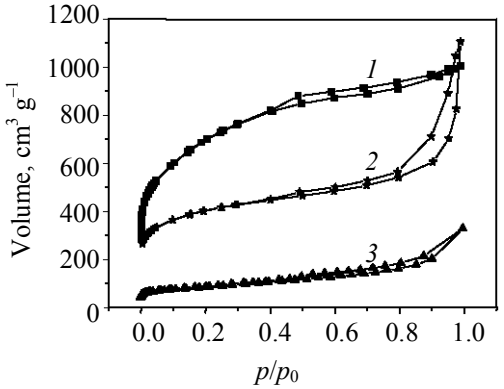

Fig. 1. Nitrogen adsorption–desorption isotherms (77 K) for inverse opal (*1*, *2*) carbon and (*3*) SiC/C composite structures with the starting SiO_2 particle diameters (*1*) 10 and (*2*, *3*) 300 nm.

after which the samples were washed (in a solution of HCl and distilled water) and dried at 100°C (12 h). The carbon contents of the resulting samples were 1.5–5.0 wt %.

The porous structure characteristics of the samples were determined from the nitrogen–desorption isotherms measured at 77 K (Quantachrome QuadraWin instrument). Before measurements the samples were degassed at 300°C for 2 h under helium. The porous structure parameters were calculated by standard procedures (BET, BJH, DFT).

Helium ions were implanted into SiC/C inverse opal samples (Extrion/Varian 200-1000 implanter; He^+ energy 40 keV, doses 10^{13}–10^{15} ion/cm^2). Two series of samples with different carbon contents of the starting SiO_2/C composite (~6.5 and ~1.5 wt % before the carbothermal reduction stage). The reference sample was nanocrystalline graphite not subjected to thermal treatment. Photoluminescence was measured on a MDR-2 diffraction monochromator at room temperature by a standard phase-sensitive procedure. Photoluminescence was excited by a 325-nm helium–cadmium laser (pumping power 0.5 W cm^{-2}). The photoluminescence spectra were registered using a FEU-79 photoelectron multiplier. The structure of the samples was studied by means of a JEM-2100 transmission electron microscope.

RESULTS AND DISCUSSION

Effect of Thermochemical Treatment of Opal Templates on the Porous Structure of Composites

Figure 1 shows the adsorption–desorption isotherms of three samples: carbon composite (two samples) and carbon–silicon carbide composite (SiC/C) with inverse opal structure.

The samples were subjected to thermal treatment at a high temperature and then activated with potassium hydroxide at 1070 K. Conditions of thermal treatment: 1770 K, 2 h, vacuum (SiC/C composite); 1200 K, 2 h (inverse opal, initial SiO_2 particle diameter 300 nm); and 900 K, 2 h (inverse opal, initial SiO_2 particle diameter 10 nm).

The isotherms were assigned type II according to the classification [1], which implies polymolecular adsorption. The sorption hysteresis loop is close to the relative pressure point p/p_0= 0.4, implies prevalence of micropores (<2 μm).

The porous structure parameters of the SiC/C–inverse opal and C–inverse opal composites are listed in the table. The SiC/C–opal systems are formed at a high-temperature treatment (1770 K), when silicon carbide is synthesized in part by carbothermal reduction of SiO_2. The C–opal systems were treated at 1200 K and 900 K, when SiC is not formed. Comparison of the

Porous structure parameters of inverse opal carbon and SiC/C nanocomposites after thermochemical treatment

Composite	SiO_2 particle diameter, nm	Treatment temperature, K	Specific surface area, m^2 g^{-1}	Specific pore volume, cm^3 g^{-1}	Specific micropore volume, cm^3 g^{-1}	Pore diameter, nm
SiC/C–opal	300	1770	180	0.57	–	3.64
SiC/C–opal. activated	300	1770	294	0.51	0.32	1.1; 3.85
	73	1770	2.65	–	–	1.9
C–opal	300	1200	570	0.70	0.62	1.06; 3.6
	73	1200	430	0.60	0.4	1.8; 10
C–opal. activated	300	1200	1448	1.72	1.41	1.2; 3.6
	12	900	2050	0.99	0.89	1.23; 3.5
	10	900	2478	1.6	1.4	0.98; 3.5

resulting data reveals a clear dependence of porosity on the diameter of the starting silicon dioxide particles and the carbonization temperature.

The specific surface area of the composites increases with decreasing SiO_2 particle size and treatment temperature. This correlation is confirmed by the fact that an increase of the treatment temperature leads to agglomeration of nanoparticles, an increase of the fraction of macro- and mesopores and, as a result, a decrease of the specific surface area. The temperature effect is the most evident in the case of small SiO_2 particles.

Thus, the key factors controlling the specific surface area (by BET) of carbon and carbon–silicon carbide nanocomposites with inverse opal structure are the temperature of thermochemical treatment and the size of the starting silicon dioxide particles. Alkaline activation, too, strongly affects the porous structure of composites. Thus, the specific surface area and pore volume of activated and unactivated C–opal samples differ 3 and 2.5 times, respectively.

Structure of SiC/C Inverse Opal

Transmission electron microscopy of the SiC/C composites revealed in their structure, along with SiC, graphite, and amorphous carbon crystallites, spherical carbon particles including concentric graphite-like shells (onion-like) (Fig. 2). The onion-like particles were purposefully prepared by exposure of carbon materials to electrons in the electron microscope column [1]. Such structure was previously observed by Ugarte [2].

As shown in [3–6], high-temperature treatment of diamond particles gives rise to onion-like particles formed by fullerene-like spheres placed one inside the other. As such particles heated to 700°C and exposed to electrons, their nuclei can transform into diamond [7]. The interplanar spacing in the irradiated particles (onions) decreases in going from outer to inner shells from 0.34 to 0.22 nm. The decrease of the interplanar spacing is explained by contraction of the irradiated particle, which leads to diamond formation in its nucleus. According to estimates in [7], the pressure inside the particle may be even higher than the equilibrium pressure of the graphite–diamond transition. The formation of diamond nuclei was previously observed in many onion-shaped particles having more than 15 shells. The size of crystalline diamond nuclei varies from 2 to 50 nm. However, at room temperature the irradiated particle lattice destroys because of numerous defects like interfaces which adversely affect stability of onions [1].

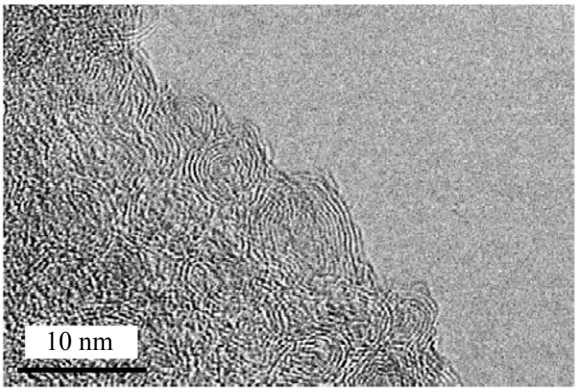

Fig. 2. High-resolution TEM image of a part of the SiC/C composite sample, containing onion-like particles.

In one of twenty different sites of the sample we observed a giant onion-like particle ~100 nm in diameter. Probably, such a giant onion particles is formed at the site of an octahedral void in the opal lattice, which is fully filled with carbon, since the diameter of the octahedral void is 0.42 $D(SiO_2)$, where $D(SiO_2)$ is the diameter of a SiO_2 sphere. In the present work we dealt with opals with $D(SiO_2) \sim 260$ nm. The diameter of octahedral pores in this material corresponds to an inscribed sphere ~ 100 nm in diameter.

Analysis of the results of measurements in numerous sites of the inverse opal nanocomposite showed that the typical diameter of the onion-like particles was ~10 nm. The diameter of the nucleus in such a particle is ~2 nm, which is consistent with data in [7].

Helium Ion Implantation-Induced Photoluminescence of SiC/C Nanocomposites

A typical photoluminescence spectrum of the starting SiC/C inverse opal sample (Fig. 3, curve *1*) looks like a broad band in the range 3.5–1.9 eV (350–650 nm) with several unresolved maxima. For the sake of comparison in Fig. 3 (curve *2*) we show the spectrum of the carbon–opal composite before silicon dioxide was removed from it by etching in hydrofluoric acid. After etching the spectrum changed only slightly. The broad band with a maximum at 2.8–3.2 eV was prevailing in both spectra.

The role of photoluminescence sources in SiC/C nanocomposites can be played both by SiC particles,

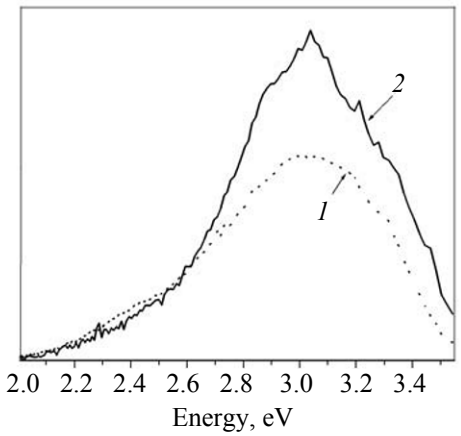

Fig. 3. Typical photoluminescence spectra of the (*1*) starting inverse opal sample and (*2*) SiC/C composite before removal of SiO_2.

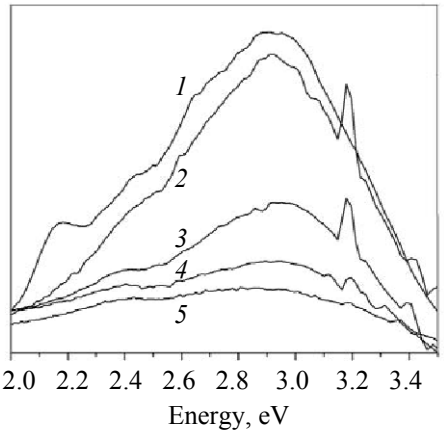

Fig. 4. Photoluminescence spectra of the (*1*) starting inverse opal SiC/C composite (after HF etching) and samples annealed under oxygen for (*2*) 15, (*3*) 38, and (*4*) 106 h at 500°C and (*5*) 106 h at 500°C plus 25 h at 700°C.

as well as by SiO_2 particles remaining after HF etching. It is not excluded that carbon quantum dots which are present in the material [9–12] and defects in SiO_2 with carbon admixture can also function as luminescence centers [8, 13–16]. The photoluminescence spectra of certain samples cut out from the composite bulk showed a band at 2.15 eV (575 nm) (Fig. 4, curve *1*).

In view of the fact that this band disappeared after carbon had been removed from the composite by annealing in oxygen [17], we studied a series of samples obtained by annealing a single starting composite sample at 500 and 700°C with the aim to find out the contribution of different luminescence centers into the spectrum of the composite. Figure 4 presents the photoluminescence spectra of this series of samples: the starting composite sample and the same sample annealed under oxygen consecutively for 15 h, 23 h, and 68 h at 500°C and for 25 h at 700°C. The spectrum of the composite after the first annealing no longer contains the band at 2.15 eV (575 nm) and acquires a narrow peak at 3.18 eV; apart from that, the spectrum is similar to that the starting sample before removal of carbon. Thus, the band at ~ 2.15 eV (575 nm) can be assigned to carbon clusters in the composite. According to [18], the luminescence at ~ 570 nm is associated with the presence of nanocrystals containing sp^3-bonded carbon, and the intensity of this band correlates with the number of these bonds.

The peak at 3.18 eV (390 nm) suggests that the sample contains 4H polytype SiC crystals, which agrees with the results in [19]. This peak is faintly visible in the spectrum of the starting opal–carbon composite before its HF etching (Fig. 3, curve *2*). After etching, the spectra of the samples cut out from the composite bulk no longer show the peak at 3.18 eV (Fig. 4, curve *1*). This result can be explained by a low (~1%) fraction of silicon carbide in the sample depth [17]. However, the residue freed from carbon by annealing contains amorphous SiO_2 and crystalline SiC (X-ray phase analysis data); therewith, the fraction of SiC in the residue is much higher, as evidenced by a well-defined peak in the photoluminescence spectrum (Fig. 4, curve *2*). In the spectra of the sample annealed under oxygen, the peak at 3.18 eV gradually attenuates until it disappears completely after annealing at 700°C (Fig. 4, curves *2–5*). Such behavior can be explained by oxidation of SiC nanocrystals ($SiC + 2O_2 = SiO_2 + CO_2$). The results of X-ray phase analysis provide evidence showing that the fraction of SiC in the sample decreases on thermal treatment.

In the spectrum of the annealed sample, we observed a strong variation in the intensity of the dominant band at 2.8–3.2 eV, and after the final annealing stage the spectrum looked like two broad bands at 2.4 and 2.7–3.1 eV. In many works [8, 13–16, 20–24], the luminescence in the range 2.7–3.1 eV is assigned to oxygen defects and carbon admixtures in SiO_2. The photoluminescence decay at 2.7–3.1 eV is naturally associated with a decrease in the number of defect centers after thermal treatment under oxygen. Long-term thermal treatment (> 130 h) did not result in the elimination of all defects: A weak band at 2.7–3.1 eV was still observed. Probably, during thermal treatment a part of $C–SiO_2$ centers remains inacces-

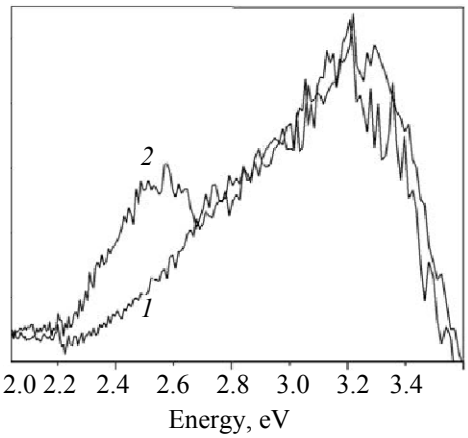

Fig. 5. Photoluminescence spectra of the same SiC/C sample from the first series, measured (*1*) before and (*2*) after He^+ implantation. He^+ energy 40 keV, dose 1×10^{15} ion/cm^2.

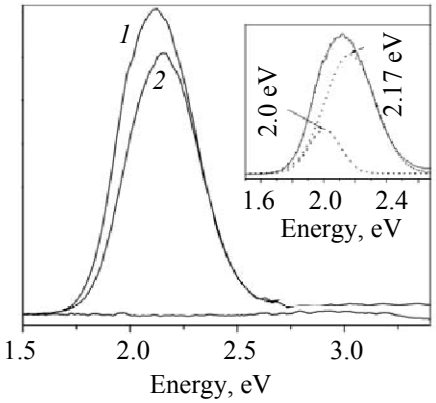

Fig. 6. Photoluminescence spectra of (*1*, *2*) two typical orange-red luminescing dots (ORD) and (*3*) a part of the sample containing no ORD. The insert shows the deconvolution of the band with a maximum at ~2.12 eV (curve *1*) into two bands with maxima at ~ 2.17 eV (571 nm) and 2.0 eV (620 nm), which are characteristic of two diamond N–V centers.

sible for oxygen due to agglomeration of SiO_2 nanoparticles around them.

The band at ~2.4 eV (517 nm) was previously observed in the spectra of SiO_2–Si–C layers obtained by silicon and carbon implantation into SiO_2 [25], as well as SiO_2–C films deposited by the plasma-chemical technology [26] and carbonization/oxidation of porous silicon [8]. The authors of these works associate the photoluminescence at 2,4 eV with the presence of SiC nanoclusters in the SiO_2 matrix. The presence of silicon carbide in our studied composites was confirmed both by X-ray phase analysis and IR spectroscopy [17]. Moreover, as shown in [19], under similar carbothermal reduction conditions of silicon dioxide, a 3C–SiC cubic polytype (along with 6H and 4H) is formed. It is known that the photoluminescence at 2.4 eV corresponds to the edge emission of the 3C–SiC cubic polytype [27].

Thus, analysis of the photoluminescence spectra of SiC/C nanocomposites before implantation of helium ions shows that the dominant emission occurs in the blue spectral range (2.8–3.2 eV) and arises from defect centers in the SiO_2 matrix, associated with oxygen vacancies and carbon admixtures. Some contribution into radiation is also made by SiC nanocrystals, and, therewith, the green part of the photoluminescence spectrum is largely associated with 3C–SiC cubic polytype nanocrystals (2.4 eV).

Let us now focus on the photoluminescence spectra of He^+-implanted samples. As seen from Fig. 5, the spectrum of a thermally untreated implanted sample contains, like the photoluminescence spectrum of an unimplanted sample, a weak band in the blue-green range at 3.1–2.5 eV (400–500 nm). Annealing after implantation at 800°C in an inert atmosphere leads to the appearance of local dots (less than 1 mm) with an orange-red luminescence. The observed changes in the spectrum are associated with the appearance of a broad band at 2.15 eV (575 nm), which is analogous to the band in curve *1* in Fig. 2. However, the band in the spectrum in Fig. 5 contains a well-defined shoulder near 1.95 eV (635 nm).

One of the samples of the second series, annealed at 800°C, contained five local dots on a square of about 1 cm^2, which emitted an orange-red light under UV laser radiation. The luminescence spectra of two typical dots are shown in Fig. 6 (curves *1* and *2*). The blue luminescence intensity measured at the sample part containing no dots emitting an orange-red light (curve *3*) was almost two orders of magnitude lower compared to the intensity of the orange-red luminescence of the second-series sample. It should be noted that orange-red dots were found in only one of the four samples of the second series.

The band with a maximum at ~ 2.16 eV (574 nm) (Fig. 6, curve *2*) and the half-width of 0.40 eV is analogous to the band in curve *4*, Fig. 3, which was also observed in [17]. The spectrum of the second orange-red dot (curve *1*) is a broader band at ~2.12 eV (585 nm), which can be deconvoluted (see the insert in Fig. 6) into two bands with maxima at ~ 2.17 eV (571 nm) and 2.0 eV (620 nm). Such bands are

characteristic of two types of diamond N–V centers: a neutral $(N–V)^0$ center (575 nm) and a negatively charged $(N–V)^–$ center (638 nm) [28, 29].

The shift of the maxima and the large band width point to small-sized photoluminescence centers like nanodiamods (5 nm) [30]. We found that these photoluminescence centers are instable in time. After about several months these orange-red luminescing dots disappeared from the studied samples. It should be noted that the reference samples exposed to He^+ irradiation did not acquire orange-red luminescence.

ACKNOWLEDGMENTS

The work was financially supported by the Russian Foundation for Basic Research (project. no. 10-02-00460).

The authors are grateful to E.N. Kabachkov for help in mesuring adsorption isotherms and N.S. Sukhinina for sample preparation.

REFERENCES

1. Brunauer, S, Deming, L.S., Deming, W.E., and Teller, E., *J. Am. Chem. Soc*., 1940, vol. 62, p. 1763.
2. Ugarte, D., *Nature*, 1992, vol. 359, p. 707.
3. Iijima, S., *J. Crystal Growth*, 1980, vol. 5, p. 675.
4. Kuznetsov, V.L., Chuvilin, A.L., Moroz, E.M., Kolomiichuk, V.N., et al., *Carbon*, 1994, vol. 32, p. 873.
5. Kuznetsov, V.L., Chuvilin, A.L., Butenko, Y.V., Mal'kov, I.Yu., and Titov, V.M., *Chem. Phys. Lett*., 1994, vol. 222, p. 343.
6. Kuznetsov, V.L., Zilberberg, I. L., Butenko, Yu. V., Chuvilin, A. L., and Segall, B., *J. Appl. Phys*., 1999, vol. 86, p. 863.
7. Butenko, Yu.V., Kuznetsov, V. L., Chuvilin, A. L., Kolomiichuk, V. N., et al., *J. App. Phys*., 2000, vol. 88, p. 4380.
8. Banhart, F. and Ajayan, P.M., *Nature*, 1996, vol. 382, p. 433.
9. Liu, H., Ye, T., and Mao, C., *Angew. Chem. Int. Ed*., 2007, vol. 46, p. 6473.
10. Liu, R.L., Wu, D.Q., Liu, S.H., Koynov, K., et al., *Ibid*., 2009, vol. 48, p. 4598.
11. Liu, Y., Liu, C.-Yan, and Zhang, Zh.-Y., *J. Colloid Interface Sci*., 2011, vol. 356, p. 416.
12. Wei, Y., Liu, Y., Li, H., He, X., et al., *Ibid*., 2011, vol. 358, p. 146.
13. Kontkiewicz, A. J., Kontkiewicz, A. M., Siejka, J., Sen, S., et al., *Appl. Phys. Lett*., 1994, vol. 65, p. 1436.
14. Koyma, H., *J. Appl. Phys*., 1980, vol. 51, p. 2228.
15. Sagawa, N. and Uchino, T., *Appl. Phys. Lett*., 2005, vol. 87, 251923.
16. Shi, L., Wang, Q., Li, Y., Xue, Ch., and Zhuang, H., *Appl. Surf. Sci*., 2006, vol. 252, p. 8224.
17. Emel'chenko, G.A., Masalov, V.M., Zhokhov, A.A., Maksimuk, M.Yu., et al., *Phys. Solid State*, 2011, vol. 53, no. 6, p. 1121.
18. Karavanskiy, V.A., Mel'nik, N.N., and Zavaritskaya, T.N., *Pis'ma Zh. Eksp. Teor. Fiz*., 2001, vol. 74, p. 204.
19. Zhokhov, A.A., Masalov, V.M., Matveev, D.V., Maksimuk, M.Yu., et al., *Phys. Solid State*, 2009, vol. 51, no. 8, p.1723.
20. Kong, D., Zhang, C., Xu, G., Li, G., et al., *J. Colloid Interface Sci*., 2010, vol. 352, p. 278.
21. Shen, J.L., Chen, P.N., Lee, Y.C., Cheng, P.W., and Cheng, C.F., *Solid State Commun*., 2002, vol. 122, p. 65.
22. Yu, D.P., Hang, Q.L., Ding, Y., Zhang, H.Z., et al., *Appl. Phys. Lett*., 1998, vol. 73, p. 3076.
23. Kortov, V.S., Zatsepin, A.S., Gorbunov, S.V., and Murzakaev, A.M., *Phys. Solid State*, 2006, vol. 48, no. 7, p. 1273.
24. Nishikawa, H., Shiroyama, T., Nakamura, R., Ohki, Y., et al., *Phys. Rev. B: Condensed Matter*, 1992, vol. 45, p. 586.
25. Perez-Rodriguez, A., Gonzalez-Varona, J., Garrido, B., Pellegrino, P., et al., *J. Appl. Phys*., 2003, vol. 94, p. 254.
26. Seo, S.-Y., Cho, K.-S., and Shin, J.H., *Appl. Phys. Lett*., 2004, vol. 84, p. 717.
27. Orlov, L.K., Drozdov, Yu.N., Alyabina, N.A., Ivina, N.L., Vdovin, V. I., and Dmitruk, I. N., *Phys. Solid State*, 2009, vol. 51, p. 474.
28. Davies, G. and Hamer, M.F., *Proc. Roy. Soc. Lond. A*, 1976, vol. 348, p. 285.
29. Chang, Y.-R., Lee, H.-Y., Chen, K., Chang, C.C., et al., *Nature Nanotech*., 2008, vol. 3, p. 284.
30. Bradac, C., Gaebel, T., Naidoo, N., Sellars, M.J., Twamley, J., Brown, L.J., Barnard, A.S., Plakhotnik, T., Zvyagin, A.V., and Rabeau, J.R., *Ibid*., 2010, vol. 5, p. 345.